### Title

Translation inhibition reveals interaction of 2'-deoxy and 2'-O-methyl molecular beacons with mRNA targets in living cells.




### Journal

Nucleic acids research, 37(15)

### ISSN

0305-1048



### Authors

Nitin, Nitin
Rhee, Won Jong
Bao, Gang



### Publication Date

2009-08-01

### DOI

10.1093/nar/gkp517

Peer reviewed

*Published online 15 June 2009* *Nucleic Acids Research, 2009, Vol. 37, No. 15* ***4977–4986***
*doi:10.1093/nar/gkp517*

# Translation inhibition reveals interaction of 2′-deoxy and 2′-*O*-methyl molecular beacons with mRNA targets in living cells

**Nitin Nitin, Won Jong Rhee and Gang Bao***

Department of Biomedical Engineering, Georgia Institute of Technology and Emory University, Atlanta, GA 30332, USA

Received March 11, 2009; Accepted May 30, 2009

## ABSTRACT

**Understanding the interaction between oligonucleotide probes and RNA targets in living cells is important for biological and clinical studies of gene expression *in vivo*. Here, we demonstrate that starvation of cells and translation inhibition by blocking the mTOR or PI-3 kinase pathway could significantly reduce the fluorescence signal from 2′-deoxy molecular beacons (MBs) targeting K-ras and GAPDH mRNAs in living cells. However, the intensity and localization of fluorescence signal from MBs targeting nontranslated 28S rRNA remained the same in normal and translation-inhibited cells. We also found that, in targeting K-ras and GAPDH mRNAs, the signal level from MBs with 2′-*O*-methyl backbone did not change when translation was repressed. Taken together, our findings suggest that MBs with DNA backbone hybridize preferentially with mRNAs in their translational state in living cells, whereas those with 2′-*O*-methyl chemistry tend to hybridize to mRNA targets in both translational and nontranslational states. This work may thus provide a significant insight into probe design for detection of RNA molecules in living cells and RNA biology.**

## INTRODUCTION

The ability to detect, localize, quantify and monitor the expression of specific genes in living cells in real time will offer unprecedented opportunities for advancement in molecular biology, disease pathophysiology, drug discovery and medical diagnostics. Current methods for quantifying gene expression employ either selective amplification (as in polymerase chain reaction (PCR) and serial analysis of gene expression (SAGE)) (1–4) or saturation binding followed by removal of the excess probes (as in microarrays) to achieve specificity. Although *in vitro* approaches provide a powerful tool for studying gene expression (5), they cannot be used to study the dynamics and localization of gene expression *in vivo*. *In situ* hybridization methods (6–8) have been used to address fundamental biological issues such as RNA localization and active transcription sites. However, these methods are not applicable when detecting gene transcripts within living cells.

Molecular beacon (MB)-based methods have been used to image endogenous RNAs in living cells (9–14). MBs are dual-labeled oligonucleotide hairpin probes with a fluorophore at one end and a quencher at the other end. Hybridization with the target nucleic acid opens the hairpin and physically separates the fluorophore from quencher, allowing a fluorescence signal to be emitted upon excitation. Recently, we were able to detect specific endogenous mRNAs and nuclear RNAs in living cells and image their localization (11,15,16). However, to quantifying gene expression in living cells with high sensitivity, we need to have a better understanding of probe–target interactions during various functional stages of RNA. In particular, we need to determine the fraction of RNA molecules in a given state that can hybridize with a particular probe design and chemistry. This information will help develop a relationship between the target RNA concentration and the fluorescent signal from beacon hybridization. To develop optimal assays for quantitative studies using MBs, we also need to gain an understanding of probe–target hybridization kinetics and thermodynamics in living cells. Answering these fundamental questions will have a significant impact on both disease detection and fundamental RNA biology studies using MBs.

In this study, we have analyzed the effect of translation inhibition on hybridization of 2′-*O*-methyl and 2′-deoxy MBs with target RNA molecules in living cells. The translational state of cells was inhibited by two approaches: (i) starvation of cells by removal of insulin and growth factors; (ii) blocking either the mTOR or the PI-3 kinase

*To whom correspondence should be addressed. Tel: +1 404 385 0373; Fax: +1 404 894 4243; Email: gang.bao@bme.gatech.edu

The authors wish it to be known that, in their opinion, the first two authors should be regarded as joint First Authors.

pathway using drug molecules (17–25). Starvation of cells by incubating them with insulin- and growth factor-free media can significantly change the gene expression profile of cells both at transcriptional and translational levels. Thus, starvation of cells has a broad physiologic effect on the gene expression profile in cells, as indicated by various high-throughput microarray studies. On the other hand, specific blockage of mTOR or PI-3 kinase pathway using pharmacologic approaches causes a more specific effect on translational activity. The mTOR pathway is responsible for sensing nutrient and cellular energy levels, thus plays a central role in translation and cell growth (18). It exerts control over the cell growth and translational machinery in response to a variety of stimuli (23,26,27) by inducing phosphorylation of multiple downstream effectors including ribosomal S6 kinase 1 (S6K1) and eukaryotic translational initiation factor 4E binding protein 1 (4E-BP1) (18,28). Rapamycin, an inhibitor of the mTOR pathway, is known to cause a rapid dephosphorylation of the 4E-BP1 which in turn inhibits the cap-dependent mRNA translation (22,25,26). The PI-3 kinase pathway is a regulator of mitogenic stimuli and growth factor-based signaling events in cells (25). Wortmannin, a furanosteroid metabolite of the fungi *Penicillium funiculosum*, *Talaromyces wortmannii*, is a specific, potent inhibitor of the PI-3 kinases (PI3Ks). It has been demonstrated that PI-3 kinase directly signals to the mTOR pathway through downstream activation of AKT (28). Both the mTOR and PI-3 kinase pathways converge on downstream effectors of the translation initiation machinery, i.e. 4E-BP-1 and the ribosomal S6 kinase (29).

MBs of 2′-*O*-methyl and 2′-deoxy backbone chemistries were used in studying probe–target interactions in living cells. 2′-*O*-methyl and 2′-deoxy oligonucleotide chemistries were chosen to represent probes with significantly different affinities for their target RNA molecules. Specifically, changes in oligonucleotide probe backbone chemistry from 2′-deoxy to 2′-*O*-methyl typically increase the affinity of the probe for the target and thus increase the melting temperature of the hybridized RNA–probe duplexes. These changes (increase in affinity and melting temperature) typically lead to a decrease in the off-rate of MBs hybridized to the target RNA molecules and thus a more stable RNA–probe duplex. Thus, by altering ODN probe backbone chemistry, we were able to analyze the role of probe affinity in the dynamics of probe–target interactions in living cells in response to translation inhibition.

## MATERIALS AND METHODS

### Translation inhibition

We inhibited the translational process in living cells by using rapamycin to disrupt the mTOR pathway and wortmannin to repress the PI-3 kinase pathway. For translation inhibition, we added the drug molecule of interest in the regular media and incubated cells for 40 min. For disrupting the mTOR pathway we used rapamycin (Calbiochem Corp.) at a concentration of 10 μM, and for altering the PI-3 pathway (30,31) we used wortmannin (Sigma Aldrich) at 1 μM concentration. After drug treatment, the live cells were imaged using a confocal or deconvolution fluorescence microscope.

### MB design and synthesis

MBs targeting K-ras and Glyceraldehyde 3-phosphate dehydrogenase (GAPDH) mRNAs and 28S rRNA were used in this study. Specifically, as shown in Table 1, the sequence and design of MBs used in this study for targeting GAPDH mRNA is: 5′-Cy3-CGACGGAGTCCTTCC ACGATACCACGTCG-BHQ2-3′, with the 5′-end of beacon labeled with a Cy3 dye and 3′-end labeled with a BHQ-2 quencher. The underlined bases indicate the stem sequence. The same fluorophore–quencher pair was used for MBs targeting K-ras mRNA and 28S rRNA. The beacon design for targeting K-ras mRNA is 5′-Cy3-CCT ACGCCACCAGCTCCGTAGG-BHQ2-3′ and that for targeting 28S rRNA is: 5′-Cy3-CGACTACCACCAAGA TCTGCAGTCG-BHQ2-3′.

To analyze the affinities of the MBs with their target mRNA molecules, the melting temperature of beacon/target duplexes was calculated using the Hyther Server at: http://ozone3.chem.wayne.edu/, with 200 nM concentration for beacons and RNA target, respectively. The melting temperature of MBs alone was also calculated using the mFOLD program at: http://dinamelt.bioinfo.rpi.edu/twostate-fold.php. All calculations were carried out using folding temperature of 37°C and ionic condition of 10 mM KCl and 5 mM $MgCl_2$. The results are shown in Table 1.

GAPDH-targeting beacons were synthesized with 2′-deoxy, 2′-*O*-methyl and a chimeric chemistry (with a 2′-*O*-methyl loop domain with a 2′-deoxy stem region). Beacons targeting K-ras mRNA and 28S rRNA were synthesized with 2′-deoxy chemistry only. MBs with 2′-deoxy DNA chemistry (deoxyribonucleotide backbone) were synthesized at MWG Biotech (NC, USA) and purified using double high performance liquid chromatography (HPLC). GAPDH-targeting beacons with 2′-*O*-methyl and chimeric chemistry were synthesized at Biosource Corp. (CA, USA).

### MB and RNA target hybridization kinetics

Hybridization assays were performed for three different GAPDH MBs (2′-deoxy, 2′-*O*-methyl and chimeric) with RNA targets, in which 100 nM of each MB was incubated with 200 nM of RNA targets (AAUAAUGGUAUCGUG GAAGGACUCAAAAA) in PBS buffer at room temperature. Hybridization kinetics was observed by reading fluorescent signals every 20 ms using spectrofluorophotometer (Shimadzu).

### MB delivery

For cellular delivery of MBs, normal human dermal fibroblast (HDF) cells were treated with activated streptolysin O (SLO) (Sigma Aldrich) for a period of 10 min as described previously (12) with a slight modification in the experimental procedure. Specifically, the incubation of cells with SLO and MBs was carried out in a regular serum-rich medium. We did not observe any difference in the efficiency of probe delivery in a regular media as

compared with the serum-free media used in our previous studies (12). This allowed us to maintain the same cell culture medium conditions throughout the experiment. After removing the SLO-containing medium, the cells were incubated in the regular medium for 30 min before fluorescence imaging of probe-target hybridization. The same incubation time and delivery method were used for beacons with 2′-deoxy and chimeric 2′-*O*-methyl probe chemistry. In the case of MBs with 2′-*O*-methyl backbone chemistry for both stem and loop regions (which have a much higher melting temperature compared with beacons with DNA backbone), they were incubated for ~3 h after removal of SLO in order to have sufficient hybridization with the RNA target.

### Fluorescence imaging

Most imaging experiments for detecting fluorescence signal in living cells were carried out using a confocal microscope (Zeiss Axiovert LSM-100) with an optical pin hole of 2.4 airy units with excitation at 543 nm and emission detection at 560–615 nm using a band pass filter. These optical settings were chosen to provide a thick slice in a confocal image and thus an integration of the fluorescence signal over a significant depth.

### Quantification of imaging data

Mean fluorescence intensity (MFI) for each individual cell was quantified using Adobe Photoshop 7.0. To calculate the MFI values for each individual cell, a pseudo-colored confocal image was converted to a gray scale image and a boundary region was defined around the outer cell membrane. To define a cell boundary, white light image was merged with the fluorescence image. The MFI in a defined region was calculated using image quantification tool in Adobe Photoshop. This process was repeated for both control and treated cells (based on three independent repeat experiments). Average mean fluorescence intensity for both control and treated cells was calculated and the results were normalized based on MFI of control samples.

### Immunocytochemistry of phospho-eIF4G

For phospho-eIF4G (p-eIF4G) staining, cells were fixed with 4% paraformaldehyde for 15 min followed by permeabilization with 0.2% Triton X-100. Cells were blocked with 5% goat serum in PBS for 30 min at 37°C and incubated with blocking solution containing rabbit polyclonal p-eIF4G antibody (Cell Signaling Technology) for 30 min at 37°C. After washing three times, cells were incubated with secondary antibody conjugated with Alexa Fluor 488 (Molecular Probes), Hoechst 33342 and rhodamine phalloidin (Molecular Probes) for 30 min at 37°C. Fluorescence signals in fixed cells were captured and analyzed with a DeltaVision Deconvolution Microscope (Applied Precision, Inc.).

### Real-time quantitative PCR (RT-PCR)

Total RNA was isolated from cells using Qiagen RNeasy Mini Kit. Total RNA was used for cDNA synthesis by random hexamers with Invitrogen Thermoscript Reverse Transcriptase kit. For RT-PCR, the cDNA was amplified using a Stratagene Mx3005P (Stratagene) RT-PCR machine. The Ambion's 18S primers were used as an internal control for RT-PCR. PCR amplification was performed with the following primers with 60°C for GAPDH and 53°C for K-ras as the annealing temperatures: GAPDH forward (CGA CCC ATG GCA AAT TCC ATG GCA), GAPDH reverse (TCT AGA CGG CAG GTC AGG TCC ACC), K-ras forward (GAT TCC TAC AGG AAG CAA GT) and K-ras reverse (TAA TGG TGA ATA TCT TC).

## RESULTS AND DISCUSSIONS

### MB design, melting temperature and hybridization kinetics

MBs were designed to target K-ras and GAPDH mRNAs and 28S rRNA. We chose GAPDH and K-ras mRNAs as representative target mRNAs since in our previous studies we have validated the design of MBs for targeting these mRNAs. As shown in Table 1, these MBs have Cy3 fluorophore conjugated at the 5′-end and BHQ2 quencher at the 3′-end. For each beacon design, the targeting sequence (hybridization domain) is shown in italic and the underlined bases form the stem region of a MB. Three beacon backbone chemistries were used for the GAPDH-targeting beacons: 2′-deoxy (DNA), 2′-*O*-methyl (RNA-like) and chimeric of which a 2′-*O*-methyl loop and a 2′-deoxy stem are used. In Table 1, the 2′-*O*-methyl bases are indicated by lower case letters. The rationale of using a chimeric beacon with a 2′-*O*-methyl loop domain and a 2′-deoxy stem is to address the potential issue of slow hybridization rate when 2′-*O*-methyl beacons are used in live cell studies. The calculated melting temperatures for

**Table 1.** Design of MBs and their computed melting temperature

| Beacon | Target | MB Design | $T_m$ (°C) | |
|---|---|---|---|---|
| | | | MB | Duplex[a] |
| DNA | GAPDH | 5′-Cy3-CGACG*GAGTCCTTCCACGATACCA*CGTCG-BHQ2-3′ | 56.2 | 77.6 |
| RNA[b] | GAPDH | 5′-Cy3-cgacg*gagtccttccacgatacca*cgtcg-BHQ2-3′ | 56.2[c] | 84 |
| Chimeric | GAPDH | 5′-Cy3-CGACG*gagtccttccacgatacca*CGTCG-BHQ2-3′ | 56.2[b] | 84 |
| DNA | K-ras | 5′-Cy3-*CCTACGCCACCAGCTCC*GTAGG-BHQ2-3′ | 57.9 | 84.1 |
| DNA | 28S | 5′-Cy3-CGACT*ACCACCAAGATCTGC*AGTCG-BHQ2-3′ | 47.6 | 72.7 |

[a]Melting temperature was calculated for MBs with RNA targets.
[b]MBs with 2′-*O*-methyl backbone, which is RNA-like. The 2′-*O*-methyl bases are indicated by lower case italic letters.
[c]Melting temperature was calculated assuming DNA backbone for MBs.

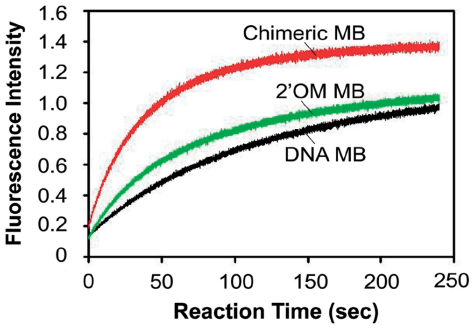


**Figure 1.** Comparison of hybridization kinetics of chimeric, 2′-*O*-methyl and 2′-deoxy MBs with short RNA targets.

MB/RNA target duplexes and for MBs alone are also shown in Table 1. As expected, for GAPDH-targeting beacons with short RNA targets, the predicted melting temperature of the hybridization domain (duplex formed by hybridization of MB loop region with RNA target) of 2′-*O*-methyl beacon is ~7°C higher than that of 2′-deoxy beacon, even without the effect of the stem region. Table 1 also gives the melting temperature of the stem loop MB alone without a hybridization target. Note that the melting temperature for 2′-*O*-methyl and chimeric beacons without target was calculated assuming DNA backbone in mFOLD (http://dinamelt.bioinfo.rpi.edu/twostatefold.php), since the program does not allow mixed backbone chemistry, and the RNA fold does not give the correct MB conformation.

To quantify the probe/target hybridization kinetics, we performed *in vitro* kinetic measurements of MBs with different backbone chemistries hybridizing to short RNA targets. The results are shown in Figure 1. These results indicate that MBs with the chimeric chemistry have much faster kinetics as compared with 2′-*O*-methyl and 2′-deoxy MBs. This is due to the higher affinity of 2′-*O*-methyl hybridization domain for target RNA as compared with 2′-deoxy hybridization domain and the low stability of the 2′-deoxy stem as compared with 2′-*O*-methyl stem. Surprisingly, 2′-*O*-methyl beacons have similar hybridization kinetics *in vitro* compared with the 2′-deoxy MBs. We believe that, for 2′-*O*-methyl beacons, the higher affinity of the hybridization domain to RNA target is counterbalanced by the higher stability of the stem.

### Cell starvation decreased signal from MBs

Serum and insulin starvation treatment have been used to repress the transcriptional and translational processes in living cells (21,32). Using this biochemical approach, we have evaluated the interaction between MBs and target mRNAs. Figure 2A and B shows the initial fluorescence intensity of MBs targeting GAPDH mRNA in a single living cell and that in the same cell after 30 min of starvation, respectively. The results clearly indicate a significant decrease in fluorescence intensity of 2′-deoxy beacons upon starvation. The decrease in beacon signal upon starvation was evident in multiple cells within a field of view, as indicated in Figure 2C and D in which control cells with regular media and cells starved after initial beacon hybridization are shown, respectively. Figure 2E provides

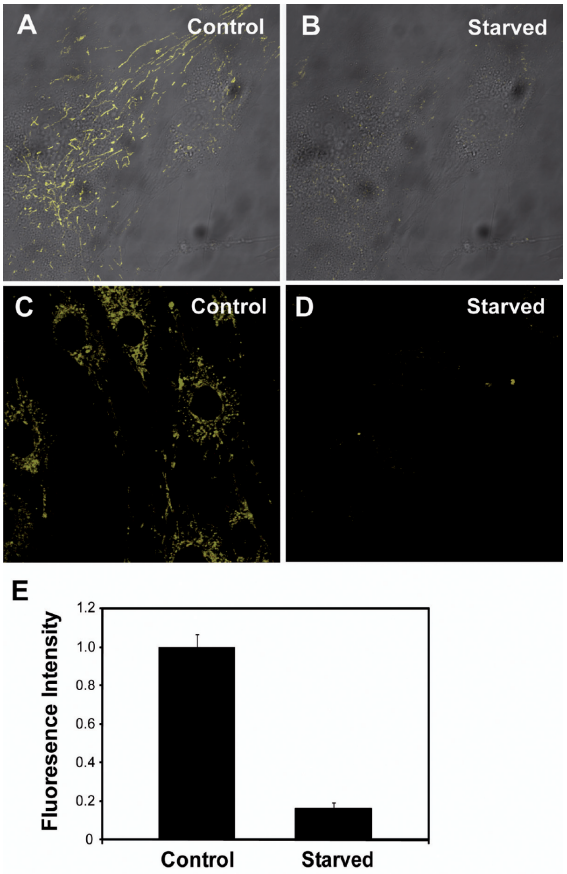


**Figure 2.** The effect of cell starvation on MB signal in detecting GAPDH mRNA in living cells. (**A**) Fluorescence signal from DNA beacons targeting GAPDH mRNA in a single HDF cell without starvation. (**B**) Fluorescence signal from GAPDH-targeting beacons in the same cell after starvation for 30 min, indicating a significant decrease in signal intensity. (**C**) Fluorescent signal from GAPDH-targeting MBs in a number of cells within a field of view under the same conditions as in (A). (**D**) With starvation, the fluorescence signal in multiple cells significantly decreased. (**E**) Normalized fluorescence intensity of MBs targeting GAPDH mRNA upon starvation compared with a control. Normalization was based on fluorescence intensity of control cells.

a quantitative representation of change in fluorescence intensity of MB targeting GAPDH mRNA upon starvation. The results indicate that there is about a 5-fold decrease in mean fluorescence intensity of MB signal upon starvation as compared with control, suggesting that during starvation, most of the hybridized MBs came off the target mRNA and reformed the hairpin structure, while very few (or none) of the MBs (including the reformed ones) in the vicinity of the target could hybridize to it. In theory, the observed decrease in fluorescence signal of beacons upon cell starvation could be attributed to either fast decay of target mRNAs or changes in RNA structure that force the bound beacons to come off and reduce target accessibility. We evaluated both of these possibilities by quantifying the target RNA level before and after treatment, as well as performing specific translational suppression, as discussed below. Clearly, the observed decrease in beacon signal upon treatment could not be a result of probe degradation by nucleases in living cells (which would increase beacon signal).

It is well understood that multiple ribosomes loaded on an mRNA molecule during translation cause the opening of mRNA secondary structure (1,33), and removal of bound proteins to allow for an effective read out of the mRNA sequence for protein synthesis. Further, it has been shown that major structural changes in mRNA secondary structure occur during translation (34). These structural changes involve the formation of a lariat structure, which brings together the 3′- and the 5′ ends of an mRNA through an association of elF4G complex with a polyA-binding proteins and elF4E (34). Since the starvation treatment does not provide specific control over the cellular pathway(s) inhibiting translation, we opt to study further the underlying biology by using specific inhibitors to suppress gene translation in living cells.

### Disrupting mTOR and PI-3 kinase pathways significantly altered signal level and its localization

To understand the effect of specific translation repression on beacon–mRNA target interaction in living cells, we targeted GAPDH and K-ras mRNAs using MBs with DNA backbone designed in our previous studies (11,12). Following SLO-based delivery and a 30-min incubation to allow beacons to hybridize to their K-ras or GAPDH mRNA target, the HDF cells were treated with either rapamycin (10 μM concentration) or wortmannin (1 μM concentration) for 40 min to suppress the mTOR and PI-3 kinase pathways, respectively. To confirm that these treatments inhibited translation in cells, we carried out immunostaining of p-eIF4G protein in rapamycin- and wortmannin-treated HDF cells, respectively. Displayed in Figure 3 are the fluorescence images in untreated (Figure 3A), starved (Figure 3B), rapamycin- (Figure 3C) and wortmannin-treated (Figure 3D) HDF cells where the signal from Alexa 488-labeled antibody targeting p-eIF4G proteins is shown in green, the cell nuclei stained by Hoechst 33342 are in blue and the F-actin filaments stained by phalloidin are in red. The results showed that the level of p-eIF4G drastically decreased after each treatment compared with control (untreated) cells, indicating that translation was blocked after the treatments (Figure 3). Therefore, in our assays, starvation, rapamycin and wortmannin treatments were all effective in inhibiting translation.

The results of the specific treatments on signals from GAPDH- and K-ras-targeting MBs are shown in Figure 4 in which fluorescence images of treated and untreated HDF cells are displayed. It is clear that, without (or prior to) treatment, signal from GAPDH beacon is distinctly localized in the cytoplasm (Figure 4A), in agreement with our previous observations (11). With rapamycin treatment, however, there was a significant decrease in the signal level similar to that observed with starvation of cells (Figure 4). As demonstrated in Figure 4B, we could only detect low levels of fluorescence signal from GAPDH mRNAs in the peri-nuclear region of treated cells, in sharp contrast to the fluorescence signal in control cells shown in Figure 4A. Displayed in Figure 4C is the result of wortmannin treatment under similar incubation conditions as for rapamycin treatment, showing similar changes

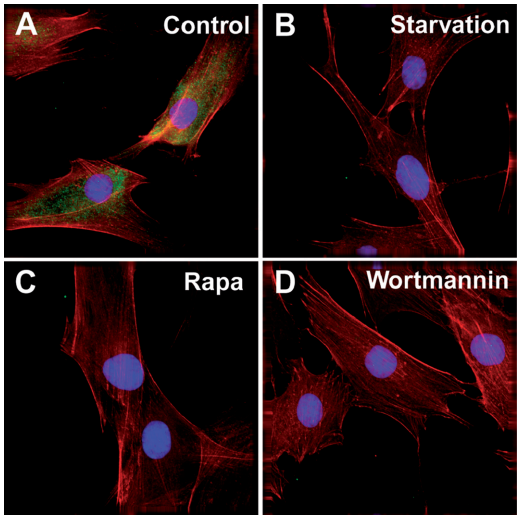


**Figure 3.** Immunostaining of p-eIF4G protein in rapamycin- and wortmannin-treated HDF cells. The fluorescence images in untreated (**A**), starved (**B**), rapamycin-treated (**C**) and wortmannin (**D**)-treated HDF cells demonstrate that the level of p-eIF4G decreased significantly after each treatment compared with control (untreated) cells, indicating that starvation, rapamycin and wortmannin treatments were all effective in inhibiting translation. In (A–D), the signal from Alexa 488-labeled antibody targeting p-eIF4G proteins is shown in green, the cell nuclei stained by Hoechst 33342 are in blue and the F-actin filaments stained by Phalloidin are in red.

(both intensity and distribution) in the fluorescence signal from GAPDH-targeting MBs in the cytoplasm as compared with that in Figure 4B. Note that the images of Figure 4A–C were taken under the same optical imaging settings. These results suggest that MBs, which were hybridized with target mRNAs before treatment, came off the target during or after treatment with rapamycin or wortmannin and formed a closed, nonfluorescent stem loop hairpin structure.

To determine if the results shown in Figure 4A–C is limited to GAPDH mRNA, we further studied the effect of translation inhibition on K-ras mRNA in living cells using MBs. Shown in Figure 4D–F are the fluorescence images of K-ras-targeting MBs (together with white light image of the cells) in control (untreated) (Figure 4D), rapamycin- (Figure 4E) and wortmannin-treated (Figure 4F) HDF cells, respectively, indicating that, upon treatment with rapamycin and wortmannin, there was a significant decrease in the fluorescence signal from K-ras-targeting beacons, similar to that shown in Figure 4A–C for GAPDH mRNAs. Quantitative measurement of changes in the fluorescence signals was carried out, indicating a greater than 5-fold decrease in fluorescence intensity of MBs targeting GAPDH and K-ras mRNAs, respectively, upon treatment with rapamycin and wortmannin, as shown in Figure 4G and F. The overall trend observed with these treatments is similar to the results obtained from starvation of cells.

The results in Figure 4A–H clearly indicate that for GAPDH and K-ras mRNAs, the fluorescence signal from MBs changes with the state of the target mRNA molecule. Specifically, translation inhibition using rapamycin or wortmannin resulted in a significant decrease

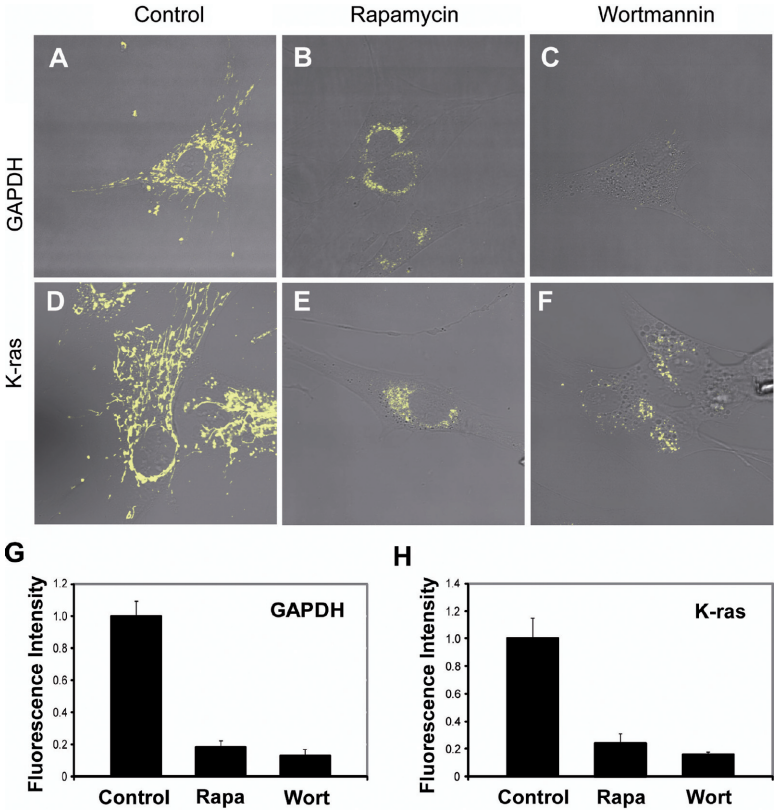


**Figure 4.** The effect of rapamycin- and wortmannin-induced translation inhibition on MB signal in targeting GAPDH and K-ras mRNAs. (**A**–**C**): Fluorescence signals from MBs in detecting GAPDH mRNAs in (A) control (untreated), (B) rapamycin-treated and (C) wortmannin-treated living cells indicate that translation inhibition significantly decreases signal from beacons. Note that fluorescence signal in treated cells is in the peri-nuclear region only, in sharp contrast to that in untreated cells. (**D**–**F**): Similar results were observed from MBs targeting K-ras mRNA in (D) untreated, (E) rapamycin-treated and (F) wortmannin-treated living cells. (**G** and **H**): Normalized fluorescence intensity of signal from MBs targeting GAPDH and K-ras mRNAs upon treatment with rapamycin and wortmannin, as compared with the control. Normalization was based on fluorescence intensity of control cells.

in fluorescence signal from MBs. It is possible that MBs coming off the target mRNA and reforming the hairpin structure could not re-hybridize to the target nor could other beacons near the mRNA target when the translation processes are repressed in cells, suggesting that the dynamic interaction between MBs and their mRNA targets depends critically on the state of mRNA. However, our observations also raise several important questions. For example, how does translation inhibition with rapamycin or wortmannin induce the decrease of signal from beacons? Could that be a result of mRNA degradation? Is the signal change indeed due to removal of beacons from target mRNAs? Would the same effect occur on nontranslated RNAs? How does the affinity of an MB with its target influence the fluorescence signal in response to translation inhibition? What structural changes of mRNA, if any, are induced by translation inhibition? We examined some of these questions and the results will be discussed in the following sections.

### Treatment with starvation, rapamycin, wortmannin and MB hybridization did not reduce the total mRNA level

The significant decrease in MB signal after translation inhibition as demonstrated in Figures 2 and 4 raises several possibilities. The reduction in beacon signal after translation inhibition by cell starvation or using rapamycin/wortmannin treatment may be a result of: (i) rapid decay of mRNAs, (ii) changes in the ribonucleoprotein (RNP) structure/composition. In both cases, an MB hybridized to an mRNA target would come off and reform the hairpin structure (thus quenching the fluorophore).

In order to have a better understanding of the mechanism(s) responsible for the significant changes in beacon signal upon treatment with rapamycin, starvation or wortmannin, we performed RT-PCR studies to quantify the levels of GAPDH and K-ras mRNAs pre- and post-treatment. As illustrated in Figure 5A, the total GAPDH mRNA level as measured using RT-PCR did not decrease with rapamycin treatment, suggesting that there was no dramatic degradation of GAPDH mRNAs due to rapamycin treatment. Our PCR results indicate that the total K-ras mRNA level even slightly increased after treatment with rapamycin (Figure 5B). This increase in mRNA level can be attributed to the increase in mRNA stability with suppression of translation (35). Further, upon treatment with starvation or wortmannin, the PCR results show essentially no change or slight increase in the levels of

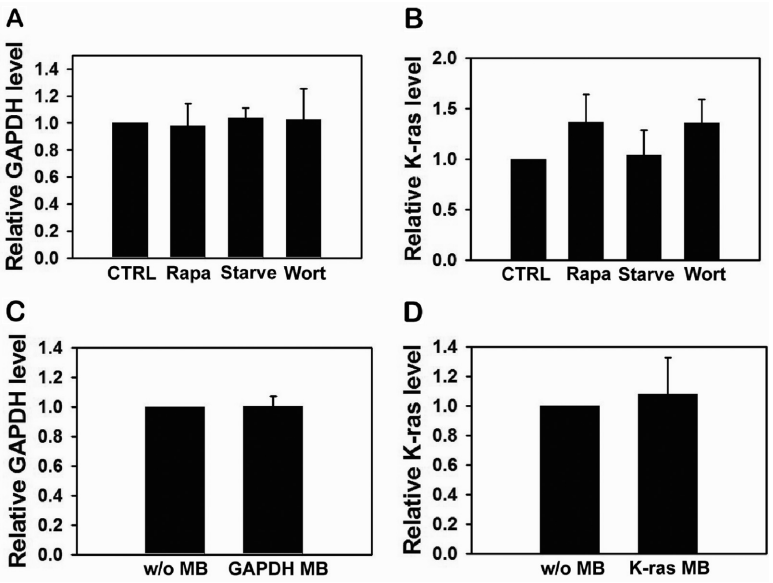


**Figure 5.** RT-PCR results for the expression of GAPDH and K-ras mRNAs in normal and translationally repressed cells (**A** and **B**) and cells with MBs delivered (**C** and **D**). (A and B): GAPDH (A) and K-ras (B) mRNA expression levels in rapamycin-treated, starved and wortmannin-treated cells as compared with that in control (untreated) cells, respectively. The results indicate that there was no reduction in GAPDH and K-ras mRNA levels after each treatment. (C and D): GAPDH (C) and K-ras (D) mRNA expression levels before and 1 h after delivery of 1 μM of GAPDH and K-ras MBs, respectively. The results indicate that MB hybridization did not affect the target mRNA level.

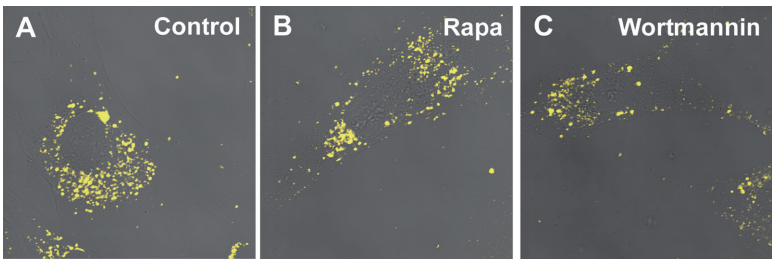


**Figure 6.** Detection of 28S rRNA in living cells as a control using MBs with 2′-deoxy backbone. (**A**) Fluorescence image of 28S rRNA localization in untreated cells. (**B** and **C**): Fluorescence images of 28S rRNA in living cells with rapamycin (B) and wortmannin (C) treatment, indicating that translation inhibition has no effect on the localization of 28S rRNAs. This observation suggests that the observed changes in MB signal upon translation inhibition are specific to GAPDH and K-ras mRNAs and does not have any significant effect on hybridization of beacons with nontranslated RNA molecules.

GAPDH and K-ras mRNAs, respectively, as compared with that of untreated cells. The results of our RT-PCR studies clearly suggest that the total mRNA levels of GAPDH and K-ras did not decrease upon treatment with rapamycin, starvation or wortmannin, ruling out the fast mRNA decay hypothesis. We also validated the presence of target mRNAs using *in situ* hybridization in fixed cells with and without treatment (data not shown).

We have also determined whether the GAPDH and K-ras MBs would induce target mRNA degradation, since anti-sense oligonucleotide with DNA backbone can induce RNase H activity to degrade target mRNAs. Specifically, 1 μM of GAPDH or K-ras MBs were delivered into cells, which were then incubated for 1 h, followed by RT-PCR analysis of mRNA levels. As shown in Figure 5C and D, both GAPDH and K-ras mRNA levels were not affected by MB hybridization to their target mRNAs. Taken together, these results clearly demonstrate that the changes in fluorescence intensity of MBs targeting K-ras and GAPDH mRNA upon starvation and suppression of translation are not due to rapid degradation of target mRNAs.

### Translation inhibition did not affect fluorescence signal from MBs hybridized with 28S rRNA suggesting specificity of the treatment

To further prove that the changes in MB signal upon pharmacologic treatments are indeed due to the inhibition of translation of mRNAs, we studied the effect of rapamycin and wortmannin treatment on the signal from MBs hybridized to a nontranslated RNA in the cytoplasm of living cells. Specifically, we designed an MB to target 28S rRNA (Table 1), which is a part of the ribosomal complex but not translated. The target accessibility for the MB designed to hybridize to 28S rRNA has been well established using both FISH and live cell studies (36–38). As shown in Figure 6A, the fluorescence signal from 28S rRNA-targeting MBs in untreated control cells had a perinuclear localization and the signal was co-localized with

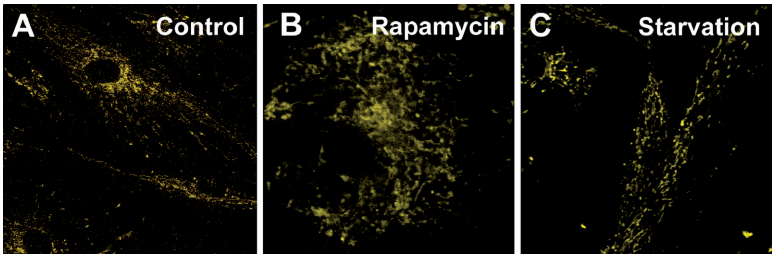


**Figure 7.** Detection of GAPDH mRNAs using chimeric (MBs with a 2′-*O*-methyl loop and a 2′-deoxy stem) (**A**) without treatment; (**B**) with rapamycin treatment; (**C**) with starvation. The results demonstrate that 2′-*O*-methyl MBs gave similar levels and distribution of fluorescence signal in treated and untreated cells. This is in contrast with results from experiments using 2′-deoxy beacons which had a significant decrease in fluorescent signal upon starvation and rapamycin treatment.

rough ER, consistent with the results obtained in our previous studies. Upon treatment with rapamycin, there was no significant change in the fluorescence signal intensity or the localization of the signal (Figure 6B). Similar results were obtained upon treatment of cells with wortmannin (Figure 6C). Therefore, we believe that the fluorescence signal from MBs targeting nontranslated RNAs (non-mRNA) is not affected by treatment with rapamycin or wortmannin. This demonstrates the high specificity of the treatment process, and clearly indicates that the changes in the translational state of GAPDH and K-ras mRNAs were responsible for the significant decrease in beacon signal upon treatment.

### Fluorescence signal from chimeric MBs and 2′-*O*-methyl MBs did not change with translation inhibition

All the results shown in Figures 2 and 4–6 were obtained using MBs with 2′-deoxy oligonucleotide backbone chemistry. As discussed above, our data suggest that upon treatment with rapamycin or wortmannin, the hybridized beacons with 2′-deoxy nucleotide chemistry came off the mRNA target, while these and other beacons in the vicinity of the mRNA could not hybridize (or re-hybridize) to the target. However, MBs with a higher affinity for RNA may interact differently with the target upon treatment. To examine if higher affinity probes such as beacons with 2′-*O*-methyl chemistry would also decrease their signal in response to specific treatments for suppressing translation, similar to the beacons with 2′-deoxy chemistry, we performed live cell imaging assays using MBs with 2′-*O*-methyl backbone and chimeric MBs (with 2′-*O*-methyl loop and 2′-deoxy stem) designed to target GAPDH mRNAs, with exactly the same probe sequence and dye–quencher pair as 2′-deoxynucleotide beacons (Table 1).

Figure 7A shows the fluorescence signal from chimeric MBs upon targeting GAPDH mRNA in living cells. The results show a similar signal level and cytoplasmic localization as obtained using 2′-deoxy oligonucleotide beacons. Similar results were obtained using GAPDH-targeting 2′-*O*-methyl MBs (data not shown). With rapamycin treatment and starvation, respectively, there was no significant decrease in the fluorescence signal (Figure 7B and C), contrary to the results obtained with the 2′-deoxy oligonucleotide beacons. This suggests that chimeric MBs with 2′-*O*-methyl hybridization loop were not competed off their target and thus remained bound to the GAPDH mRNAs even with the changes in the translational state. Based on this result, we conclude that the hybridization of 2′-*O*-methyl MBs is independent of the translational state of RNA target.

The ability of chimeric beacons with 2′-*O*-methyl hybridization loop to remain hybridized to target mRNA upon translation inhibition can be attributed to the higher affinity of these probes as indicated by the ~10–20°C increase in melting temperature of probe–RNA hybrid as compared with 2′-deoxynucleotide probes (the calculated melting temperature for probe/target duplex shown in Table 1 only reflect the effect of the loop domain, not the stem). Although the ability of chimeric and 2′-*O*-methyl MBs to detect mRNAs does not change upon translation inhibition, several issues need to be considered in using such probes for living cell mRNA detection. For example, high-affinity probes such as 2′-*O*-methyl MBs could potentially prevent the ribosomes from translating the target mRNAs. It has recently been discovered that ribosomes posses inherent helicase activity (1), which allows them to unwind the local secondary structures with melting temperatures of <70°C. However, 2′-*O*-methyl MBs could have melting temperatures close to 80°C (39,40), which may prevent the translocation of ribosomes along the target mRNA.

In summary, our results suggest that 2′-deoxy oligonucleotide beacons dissociate from the target RNA molecules when the translation process is inhibited with starvation or pharmacologic approaches, as indicated by the significant decrease in the fluorescence signal from MBs targeting GAPDH and K-ras mRNAs. With starvation and translational suppression, dissociation of MBs from target mRNAs could result from changes in RNA/protein interactions and the subsequent alteration in structure/composition of the RNP complex. These changes can thus affect the accessibility of MB for their targets. With corresponding 2′-*O*-MBs, however, no much change in beacon signal intensity was observed with translational inhibition. Further, the effect of translational inhibition on beacon–target interaction in living cells was found to be limited to mRNA molecules, with no effect on the hybridization of 2′-deoxy oligonucleotide probes to rRNA molecules. This confirms that the decrease in beacon signal was due to the changes in translational

states. Our results further suggest that the hybridization of MBs with DNA backbone to mRNA targets is favored during translation, whereas translation inhibition could prevent MBs from hybridizing to their targets. On the other hand, hybridization of 2′-*O*-methyl beacons is not affected by translational inhibition. Taken together, our findings suggest that MBs with DNA backbone hybridize preferentially with mRNAs in their translational state in living cells, whereas those with 2′-*O*-methyl chemistry tend to hybridize to mRNA targets in both translational and nontranslational states. These findings not only reveal the role of beacon backbone chemistry in the hybridization of probes to target RNA in living cells, but also reflect the complexity involved in detecting and quantifying gene expression in living cells using MBs.

## ACKNOWLEDGEMENTS

The authors thank Tashan Mistree and Brent Nix for their assistance and Phil Santangelo for helpful discussions.

## FUNDING

National Institutes of Health as a Center of Cancer Nanotechnology Excellence (CA119338); Program of Excellence in Nanotechnology (HL80711); National Institutes of Health Grant (CA103103 to G.B.). Funding for open access charge: National Institutes of Health (HL80711).

*Conflict of interest statement*. None declared.

## REFERENCES

1. Takyar,S., Hickerson,R.P. and Noller,H.F. (2005) mRNA helicase activity of the ribosome. *Cell*, **120**, 49–58.
2. Chen,X., Cheung,S.T., So,S., Fan,S.T., Barry,C., Higgins,J., Lai,K.M., Ji,J., Dudoit,S., Ng,I.O. *et al*. (2002) Gene expression patterns in human liver cancers. *Mol. Biol. Cell*, **13**, 1929–1939.
3. DePrimo,S.E., Diehn,M., Nelson,J.B., Reiter,R.E., Matese,J., Fero,M., Tibshirani,R., Brown,P.O. and Brooks,J.D. (2002) Transcriptional programs activated by exposure of human prostate cancer cells to androgen. *Genome Biol.*, **3**, RESEARCH0032.
4. Eisen,M.B. and Brown,P.O. (1999) DNA arrays for analysis of gene expression. *Methods Enzymol.*, **303**, 179–205.
5. Levsky,J.M. and Singer,R.H. (2003) Fluorescence in situ hybridization: past, present and future. *J. Cell Sci.*, **116**, 2833–2838.
6. Femino,A.M., Fogarty,K., Lifshitz,L.M., Carrington,W. and Singer,R.H. (2003) Visualization of single molecules of mRNA in situ. *Methods Enzymol.*, **361**, 245–304.
7. Femino,A.M., Fay,F.S., Fogarty,K. and Singer,R.H. (1998) Visualization of single RNA transcripts in situ. *Science*, **280**, 585–590.
8. Shav-Tal,Y., Darzacq,X., Shenoy,S.M., Fusco,D., Janicki,S.M., Spector,D.L. and Singer,R.H. (2004) Dynamics of single mRNPs in nuclei of living cells. *Science*, **304**, 1797–1800.
9. Sokol,D.L., Zhang,X., Lu,P. and Gewirtz,A.M. (1998) Real time detection of DNA.RNA hybridization in living cells. *Proc. Natl Acad. Sci. USA*, **95**, 11538–11543.
10. Tyagi,S. and Alsmadi,O. (2004) Imaging native beta-actin mRNA in motile fibroblasts. *Biophys. J.*, **87**, 4153–4162.
11. Nitin,N., Santangelo,P.J., Kim,G., Nie,S. and Bao,G. (2004) Peptide-linked molecular beacons for efficient delivery and rapid mRNA detection in living cells. *Nucleic Acids Res.*, **32**, e58.
12. Santangelo,P.J., Nix,B., Tsourkas,A. and Bao,G. (2004) Dual FRET molecular beacons for mRNA detection in living cells. *Nucleic Acids Res.*, **32**, e57.
13. Perlette,J. and Tan,W. (2001) Real-time monitoring of intracellular mRNA hybridization inside single living cells. *Anal. Chem.*, **73**, 5544–5550.
14. Santangelo,P.J. and Bao,G. (2007) Dynamics of filamentous viral RNPs prior to egress. *Nucleic Acids Res.*, **35**, 3602–3611.
15. Santangelo,P.J., Nitin,N. and Bao,G. (2005) Direct visualization of mRNA colocalization with mitochondria in living cells using molecular beacons. *J. Biomed. Opt.*, **10**, 44025.
16. Nitin,N. and Bao,G. (2008) NLS peptide conjugated molecular beacons for visualizing nuclear RNA in living cells. *Bioconj. Chem.*, **19**, 2205–2211.
17. Proud,C.G. (2004) Ras, PI3-kinase and mTOR signaling in cardiac hypertrophy. *Cardiovasc. Res.*, **63**, 403–413.
18. Gingras,A.C., Raught,B. and Sonenberg,N. (2004) mTOR signaling to translation. *Curr. Top. Microbiol. Immunol.*, **279**, 169–197.
19. Gingras,A.C., Raught,B. and Sonenberg,N. (2001) Regulation of translation initiation by FRAP/mTOR. *Genes Dev.*, **15**, 807–826.
20. Hara,K., Maruki,Y., Long,X., Yoshino,K., Oshiro,N., Hidayat,S., Tokunaga,C., Avruch,J. and Yonezawa,K. (2002) Raptor, a binding partner of target of rapamycin (TOR), mediates TOR action. *Cell*, **110**, 177–189.
21. Kim,D.H., Sarbassov,D.D., Ali,S.M., King,J.E., Latek,R.R., Erdjument-Bromage,H., Tempst,P. and Sabatini,D.M. (2002) mTOR interacts with raptor to form a nutrient-sensitive complex that signals to the cell growth machinery. *Cell*, **110**, 163–175.
22. Proud,C.G. (2004) Role of mTOR signalling in the control of translation initiation and elongation by nutrients. *Curr. Top. Microbiol. Immunol.*, **279**, 215–244.
23. Proud,C.G. (2004) mTOR-mediated regulation of translation factors by amino acids. *Biochem. Biophys. Res. Commun.*, **313**, 429–436.
24. Sarbassov,D.D., Guertin,D.A., Ali,S.M. and Sabatini,D.M. (2005) Phosphorylation and regulation of Akt/PKB by the rictor-mTOR complex. *Science*, **307**, 1098–1101.
25. Sekulic,A., Hudson,C.C., Homme,J.L., Yin,P., Otterness,D.M., Karnitz,L.M. and Abraham,R.T. (2000) A direct linkage between the phosphoinositide 3-kinase-AKT signaling pathway and the mammalian target of rapamycin in mitogen-stimulated and transformed cells. *Cancer Res.*, **60**, 3504–3513.
26. Bhandari,B.K., Feliers,D., Duraisamy,S., Stewart,J.L., Gingras,A.C., Abboud,H.E., Choudhury,G.G., Sonenberg,N. and Kasinath,B.S. (2001) Insulin regulation of protein translation repressor 4E-BP1, an eIF4E-binding protein, in renal epithelial cells. *Kidney Int.*, **59**, 866–875.
27. Preiss,T., Baron-Benhamou,J., Ansorge,W. and Hentze,M.W. (2003) Homodirectional changes in transcriptome composition and mRNA translation induced by rapamycin and heat shock. *Nat. Struct. Biol.*, **10**, 1039–1047.
28. Miron,M., Lasko,P. and Sonenberg,N. (2003) Signaling from Akt to FRAP/TOR targets both 4E-BP and S6K in Drosophila melanogaster. *Mol. Cell Biol.*, **23**, 9117–9126.
29. Miron,M., Verdu,J., Lachance,P.E., Birnbaum,M.J., Lasko,P.F. and Sonenberg,N. (2001) The translational inhibitor 4E-BP is an effector of PI(3)K/Akt signalling and cell growth in Drosophila. *Nat. Cell Biol.*, **3**, 596–601.
30. Ridderstrale,M. and Tornqvist,H. (1994) PI-3-kinase inhibitor wortmannin blocks the insulin-like effects of growth hormone in isolated rat adipocytes. *Biochem. Biophys. Res. Commun.*, **203**, 306–310.
31. Barker,S.A., Caldwell,K.K., Hall,A., Martinez,A.M., Pfeiffer,J.R., Oliver,J.M. and Wilson,B.S. (1995) Wortmannin blocks lipid and protein kinase activities associated with PI 3-kinase and inhibits a subset of responses induced by Fc epsilon R1 cross-linking. *Mol. Biol. Cell*, **6**, 1145–1158.
32. Kim,D.H., Sarbassov,D.D., Ali,S.M., Latek,R.R., Guntur,K.V., Erdjument-Bromage,H., Tempst,P. and Sabatini,D.M. (2003) GbetaL, a positive regulator of the rapamycin-sensitive pathway required for the nutrient-sensitive interaction between raptor and mTOR. *Mol. Cell*, **11**, 895–904.
33. Rozen,F., Edery,I., Meerovitch,K., Dever,T.E., Merrick,W.C. and Sonenberg,N. (1990) Bidirectional RNA helicase activity of

eucaryotic translation initiation factors 4A and 4F. *Mol. Cell Biol.*, **10**, 1134–1144.
34. Gebauer,F. and Hentze,M.W. (2004) Molecular mechanisms of translational control. *Nat. Rev. Mol. Cell Biol.*, **5**, 827–835.
35. Cougot,N., Babajko,S. and Seraphin,B. (2004) Cytoplasmic foci are sites of mRNA decay in human cells. *J. Cell Biol.*, **165**, 31–40.
36. De Rijk,P., Robbrecht,E., de Hoog,S., Caers,A., Van de Peer,Y. and De Wachter,R. (1999) Database on the structure of large subunit ribosomal RNA. *Nucleic Acids Res.*, **27**, 174–178.
37. Kalle,W.H., Macville,M.V., van de Corput,M.P., de Grooth,B.G., Tanke,H.J. and Raap,A.K. (1996) Imaging of RNA in situ hybridization by atomic force microscopy. *J. Microsc.*, **182(Pt 3)**, 192–199.
38. Politz,J.C., Tuft,R.A. and Pederson,T. (2003) Diffusion-based transport of nascent ribosomes in the nucleus. *Mol. Biol. Cell*, **14**, 4805–4812.
39. Majlessi,M., Nelson,N.C. and Becker,M.M. (1998) Advantages of 2′-O-methyl oligoribonucleotide probes for detecting RNA targets. *Nucleic Acids Res.*, **26**, 2224–2229.
40. Tsourkas,A., Behlke,M.A. and Bao,G. (2003) Hybridization of 2′-O-methyl and 2′-deoxy molecular beacons to RNA and DNA targets. *Nucleic Acids Res.*, **30**, 5168–5174.